2010 IEEE International Conference on Robotics and Automation
Anchorage Convention District
May 3-8, 2010, Anchorage, Alaska, USA

Design of a New Independently-Mobile Reconfigurable Modular Robot

Michael D.M. Kutzer, Matthew S. Moses, Christopher Y. Brown, David H. Scheidt, Gregory S. Chirikjian, and Mehran Armand

Abstract— **A new self-reconfigurable robot is presented. The robot is a hybrid chain/lattice design with several novel features. An active mechanical docking mechanism provides inter-module connection, along with optical and electrical interface. The docking mechanisms function additionally as driven wheels. Internal slip rings provide unlimited rotary motion to the wheels, allowing the modules to move independently by driving on flat surfaces, or in assemblies negotiating more complex terrain. Modules in the system are mechanically homogeneous, with three identical docking mechanisms within a module. Each mechanical dock is driven by a high torque actuator to enable movement of large segments within a multi-module structure, as well as low-speed driving. Preliminary experimental results demonstrate locomotion, mechanical docking, and lifting of a single module.**

Index Terms— **cellular and modular robots, robotics in hazardous fields, mechanism design of mobile robots**

I. INTRODUCTION

A great variety of self-reconfigurable modular robotic systems have been developed to date (see reviews of recent research in [1] and [2]). In this paper we detail the design and development of a new self-reconfigurable modular robotic system. The design of this system is tailored toward the specific application of electrical and hydraulic damage repair/mitigation in environments with limited accessibility and insufficient work space for conventional robots. In the following sections, we provide details of our new design, justification for some of the design tradeoffs performed, compare the system with other well known examples from various research groups, and discuss preliminary multi-module simulations and experiments with a prototype robot module.

The motivation for this work stems from the desire to create a system capable of damage repair/mitigation in hazardous environments. Specifically, the overarching goal of this work is to create a system that can be deployed on Navy ships. In the event of an explosion or other catastrophic incident, the envisioned system can be deployed as close as possible (without endangering crew members) to the damaged area (e.g. multiple units can be thrown into the damaged compartment). Once deployed, the system will begin rebuilding broken connections (e.g. communication, electrical, steam, hydraulic, etc.) to restore critical functionality to the ship. The system will then remain in place until permanent repairs can be made.

Self-reconfigurable modular robots (SRMRs) are often classified as chain-like [3] [4], lattice-like [5] [6], or hybrid [7] [8]. Lattice-like modular robots are arranged in three dimensional grids. Typically, the intended application for lattice-like modular robots is for reconfigurable structures such as bridges, buildings, or digital clay. Chain-like modular robots are better suited for tasks requiring high mobility. The chain-like geometry allows the modules to move with fewer self-obstructions, and to adapt configurations in response to different mobility hindrances. A variety of locomotion modes have been demonstrated. Hybrid chain/lattice systems were introduced to derive benefits from both approaches. Excellent reviews of recent research in this area can be found in [1] and [2], including comparisons of chain/lattice/hybrid architectures.

The robot presented here is hybrid, able to function in chain or lattice structures. Two of the best known hybrid designs are the MTRAN series [7] [9] [2] and Superbot [8] [10]. The geometry of MTRAN and Superbot Modules is similar, with the exception that Superbot contains an extra degree of freedom between the modules' ends. Superbot uses genderless connections, while MTRAN has developed male/female connectors based on magnetic devices [7] and actuated hook connectors [9]. The modules presented here have quite different geometry, chosen in part for the desire to make the modules independently mobile, and to allow the use of genderless connectors. Similar to the modules described in [9], our modules rely on hooked docking connections rather than magnetic connections. While magnetic connections are clearly advantageous for alignment, the strong magnetic field required to create adequate connection forces can be an encumbrance in environments that contain magnetic and/or ferromagnetic materials (such as the hull of a Navy ship).

A unique feature of our modules is their self-mobile ability, each module having three wheels and being able to negotiate flat surfaces. Wheel-like movements [11], and add-on wheel devices [10] have been demonstrated with SRMRs. To the best of our knowledge this is the first design where the connector mechanisms can operate as fully-functional wheels, and a single module can be driven independently.

This work was supported by Internal Research and Development funds provided by the Johns Hopkins University Applied Physics Laboratory and by NSF grant IIS-0915542, RI: Small:Robotic Inspection, Diagnosis, and Repair.

M. Kutzer, C. Brown, D. Scheidt, and M. Armand are with the Milton S. Eisenhower Research & Technology Development Center, Johns Hopkins University Applied Physics Laboratory, Laurel, Maryland {Michael.Kutzer, Christopher.Brown, David.Scheidt, Mehran.Armand}@jhuapl.edu

M. Moses, M. Kutzer, G. Chirikjian, and M. Armand are with the Laboratory for Computational Sensing and Robotics (LCSR), Johns Hopkins University, Baltimore, Maryland {matt.moses, mkutzer1, gregc, marmand2}@jhu.edu

II. MODULE DESIGN

This section presents the design decisions taken to create a modular robotic system with independently mobile units capable of assembling to achieve various forms of locomotion as well as creating rigid lattice structures.

The objective of the individual module design is to produce self-mobile units capable of creating both rigid assemblies and assemblies that facilitate negotiating rough/varied terrain. Design requirements include: self-mobility, active inter-module connections that do not rely on magnetic forces (as mentioned in Section I), chain/lattice hybridicity, self powered, optical and electrical interfaces between modules, and strong inter-module connections capable of supporting and lifting the mass of several modules in series as well as potential hydraulic/pneumatic pass-throughs with seals. In addition, the modules are designed to carry sensor payloads supplemental to those required for standard interaction (i.e. sensors designated for a specific task).

Existing methods of modular robot locomotion include rolling loops, inchworm movement of small assemblies, snake-like movements, and legged walking [2] [4] [12] [13]; driving on "half-cubical" wheels [11] or driving with add-on wheels [10] has also been demonstrated. Noting these as a baseline for locomotion requirements, we impose the additional requirement that our individual modules be capable of more traditional wheeled locomotion (i.e. driving on circular wheels). This requirement is added to ensure that modules retain some form of effective locomotion capability when operating as individuals. This is particularly useful in circumstances where no assemblies exist.

The lattice design requirement is rooted in a desire to cross/climb nontrivial distances/heights relying exclusively on limited anchoring points and/or satisfactory ledge/ground geometries. Giving modules the capability to form rigid lattice structures allows assemblies to create cantilevers for crossing wide gaps and towers for reaching elevated heights. Enabling small assemblies to climb along cantilevered or vertical lattice structures gives these structures the ability to grow [14]. Note that by using a well-suited lattice geometry, we both increase structural stability and strength when compared to a structure based on a single chain of modules.

A. Geometry and Interface Locations

Each module has three, homogeneous interface locations that act as both drive wheels and inter-module docking sites (see Fig. 1). Two of the wheels are aligned axially to create driving capabilities similar to that of a planar kinematic cart, as discussed in Section III-B. A third wheel is oriented with its axis orthogonal to and intersecting the axis of the coaxial pair. Driving relies predominantly on the coaxial pair of wheels, with the orthogonal wheel assisting only in select turning scenarios. The rationale behind an orthogonal wheel is seen when modules begin to form assemblies. This orthogonal degree of freedom enables pairs of two or more modules to achieve relative dock orientations spanning $SO(3)$.

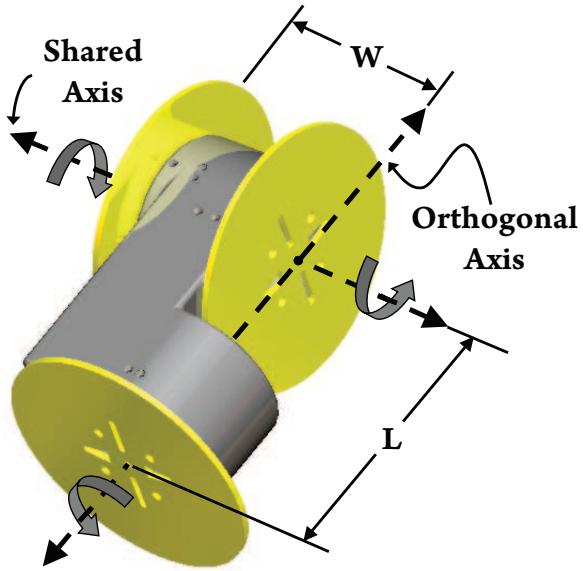

Fig. 1. Single module with axes of rotation shown.

The distance between the coaxial wheels (W) is exactly half the distance between the shared axis and the orthogonal wheel (L). In addition, the plane defined by the docking surface of the center-most coaxial wheel contains the orthogonal axis. That is, the orthogonal axis is aligned with the surface of the center-most coaxial wheel. This geometry proves advantageous when building complex structures such as a triangular prism lattice as shown in Fig. 2. In this design, W = 6.35 cm (2.5 in) and L = 12.70 cm (5.0 in).

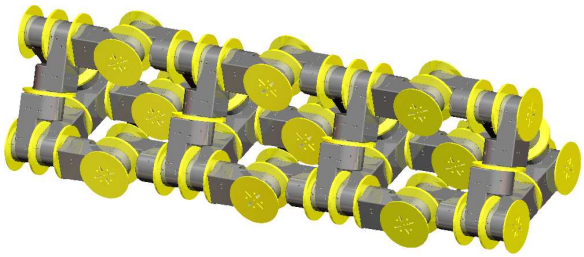

Fig. 2. 42 modules connected to form a triangular prism lattice.

Each wheel is actuated by a 24-to-1 worm gear combination allowing wheel positions to remain fixed (discounting backlash) without motor torque applied. A 3.6 V brushed DC motor (Maxon 118512) with an integrated 67-to-1 planetary gearhead (Maxon 110315) drives the worm combination. Assuming 75% efficiency of each gear train, the nominal continuous torque seen by each wheel is >2.5 Nm (22 in-lbf). The stall torque produced by this combination is >4.6 Nm (41 in-lbf). This corresponds to an ability to nominally lift 2 modules cantilevered perpendicular to the gravitational field (with a safety factor of >1.25), and 3 modules cantilevered before stalling the motor (with a safety factor of >1.00). The trade-off for this high output torque is, as always, a slow wheel speed. Under planar driving conditions, wheel speeds are approximately 4.0 rpm and

under nominal loading wheel speeds drop to 3.1 rpm.

B. Docking Mechanism

The docking connector is based on the design presented in [9]. Our docking connectors differ predominantly in that each dock is identical (i.e. connections are genderless as opposed to the male/female connectors described in [9]). Connections are created by a series of four hooks that are actuated only when making or breaking a connection. Docking surfaces (or wheel faces) can slide freely against one another when the hooks are retracted (Fig. 3a). When the hooks are extended, two hooks protrude from the surface each wheel face as shown in Fig. 3b. The ability for docking surfaces to slide freely past one another makes it possible to create many of the intricate lattice structures touched on in Section II.

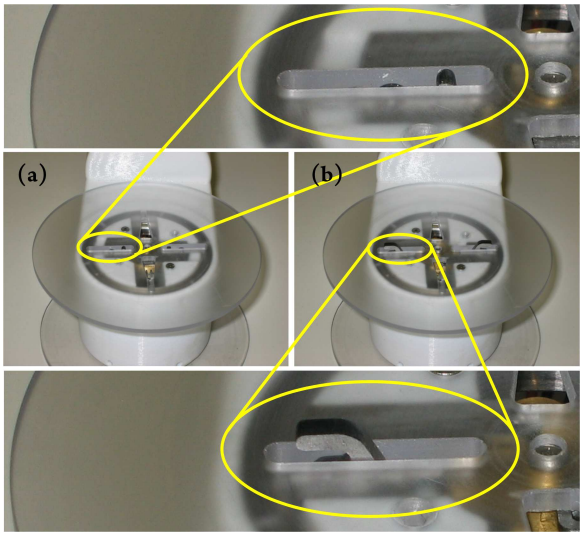

Fig. 3. Docking assembly with hooks retracted (a) and extended (d).

Docking surfaces are designed symmetrically to generate connections on 180^o intervals. While docking, two modules are required to align both in body orientation, and wheel orientation. Noting a difficulty to achieve acceptable wheel orientations when docking, docking mechanisms are designed to incorporate offset optical emitter/detector pairs, similar to those discussed in [3] and [4]. By appropriately placing these pairs, correct alignment can be tied to peaks in the detector outputs. When a proper connection is achieved, the emitter/detector pairs can be used for inter-module communication.

Due to the continuous rotation requirements for wheeled driving, docking mechanisms are electrically coupled to the module using custom slip rings. Continuous rotation slip rings have been used in other SRMRs. Modules in [11] use a commercial slip ring to allow full rotation between two halves of a single cube-shaped module. The system in [6] uses a custom built slip ring to allow full rotation between two halves of a module. In contrast to these designs, where a module is split into two pieces and the slip ring allows for relative motion between the two halves, the module presented here contains three distinct slip rings. Each slip ring allows for full rotation between a docking connector and the module chassis. The slip rings are designed to create eight independent electrical connections capable of relaying power and/or signals from the module body to the dock and vice versa. This full freedom to orient docking mechanisms proves advantageous both in making wheeled driving permissible, and in simplifying the docking process.

Fig. 4. Module shown with the center wheel removed to show slip ring.

To establish electrical connections between docked modules, the components used to extend and retract the hooks are fabricated from electrically conductive materials. By implementing conductive pads on the receiving slots of each docking surface, a single electrical connection can be established with each extended pair of hooks. When two modules connect, each can extend a pair of hooks creating two independent electrical connections between the modules. To make this an effective method of DC power transfer, these connections must be capable of switching polarity. In addition, a protocol must be implemented to ensure proper switch combinations between modules.

C. Electronic Payload and Low-level Control

The modules are powered by three 3.7V polymer lithium ion cells, providing sufficient power to drive all motors simultaneously for approximately 1.5 hrs. Under planar driving conditions, the operating life increases to $>$6 hrs. Due to multiple motors, gear trains, and structural components within each module, the volume available for drive electronics is limited. To reduce board size, the design makes use of the new line of XMega Microcontrollers from Atmel Corporation. Each module contains a single microprocessor board containing an ATXMega128A1. The chip includes integrated peripherals for reading all three of the main drive motors' quadrature encoders (Maxon 110778) in a background process, which frees up processing power for future autonomy and docking routines. The processor runs PID position and velocity control loops for each of the motors, and controls the mini docking motors through simple timed bursts of pulse-width modulated output. All motors are driven by power H-bridges (L298H) which include current-sensing outputs fed into the processor's integrated analog-to-digital converters (ADCs). The use of these ADCs further

allows the microcontroller to detect unanticipated fault conditions such as stalled or disconnected motors.

A Roving Networks RN-41 Bluetooth transceiver module enables wireless communication and control with a host computer and/or between modules. As mentioned in Section II-B, docked modules can also communicate through microprocessor controlled emitter/detector pairs located on each wheel. Each module also includes a Honeywell HMC6343 3-axis tilt-compensated magnetometer, allowing for estimation of body orientation and the future possibility of inertial navigation routines. Currently, however, module position relative to the world frame can be determined using a segmented overhead camera view. The quadrature encoders on the main drive motors also provide accurate relative position data between docked modules.

III. Kinematics

In this section, the module kinematics are described. Section III-A presents a straightforward method of defining the forward kinematics and workspace of arbitrary chain assemblies. This provides a solid foundation for future work including the formation of large and complex structures containing closed loops and trees (i.e. assemblies involving modules with connections at all three docks). Section III-B presents the driving kinematics and docking strategies for individual modules. These strategies are critical for creating assemblies from a series of individual modules.

A. Chain Assembly Kinematics

To characterize chain assemblies, each module has a frame assigned to each wheel, and a frame assigned to the center of mass. Fig. 5 illustrates frames B, P, C, and L which represent the **B**ody (also referred to as the center of mass) fixed, **P**erpendicular (also referred to as orthogonal) wheel fixed, **C**enter wheel fixed, and **L**eft wheel fixed reference frames. Wheel rotations are defined about the relative z_P, z_C, and z_L axes, with associated magnitudes of θ_P, θ_C, and θ_L respectively. To identify individual modules, subscripts are added to characters that describe a given frame (e.g. θ_{C_i} refers to the magnitude of rotation about z-axis of frame C on the i^{th} module).

Homogeneous transformations between reference frames can be described using elements of $SE(3)$. To simplify equations, the following shorthand will be used:

- $H_{B_i}^{Q_i}(\theta_{Q_i})$ - the homogeneous transformation used to convert Q_i referenced coordinates where $Q_i \in \{P_i, C_i, L_i\}$ to B_i referenced coordinates. Note that $(H_{B_i}^{Q_i}(\theta_{Q_i}))^{-1} = H_{Q_i}^{B_i}(\theta_{Q_i})$.
- D_0 - the transformation between connected wheels in a 0^o docked connection.
- D_π - the transformation between connected wheels in a 180^o docked connection.
- $R_z(\alpha)$ - rotation of angle α about the current z direction.

Using this shorthand, the transformations $H_{B_i}^{P_i}(\theta_{P_i})$, $H_{B_i}^{C_i}(\theta_{C_i})$, and $H_{B_i}^{L_i}(\theta_{L_i})$ can be defined intuitively from Fig. 5. Docking connections are defined using the transformations given in (1) and (2).

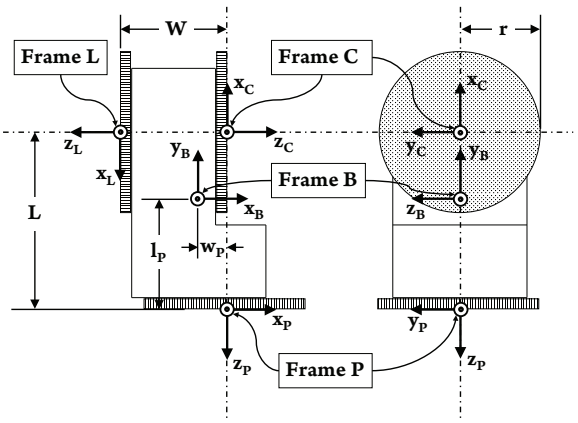

Fig. 5. Top view (left) and side view (right) of module shown illustrating the designated reference frames.

$$D_0 = \begin{pmatrix} 0 & 1 & 0 & 0 \\ 1 & 0 & 0 & 0 \\ 0 & 0 & -1 & 0 \\ 0 & 0 & 0 & 1 \end{pmatrix} \tag{1}$$

$$D_\pi = \begin{pmatrix} 0 & -1 & 0 & 0 \\ -1 & 0 & 0 & 0 \\ 0 & 0 & -1 & 0 \\ 0 & 0 & 0 & 1 \end{pmatrix} \tag{2}$$

Using these transformations, characterizing the forward kinematics of arbitrary chains can be represented using a single string of characters. For example, assuming D_π docking, the "PCπCPπCLπPCπCPπCL" chain simulated in Fig. 6 produces the transformation taking coordinates expressed in the end-effector frame (L_6) to coordinates expressed in the P_1 frame. The result is given in (3).

$$\begin{aligned} &H_{P_1}^{L_6}(\theta_{P_1}, \theta_{C_1}, \theta_{C_2}, ...\theta_{L_6}) = \\ &\quad H_{P_1}^{B_1}(\theta_{P_1}) H_{B_1}^{C_1}(\theta_{C_1}) D_\pi H_{C_2}^{B_2}(\theta_{C_2}) ... H_{B_6}^{L_6}(\theta_{L_6}) \end{aligned} \tag{3}$$

This expression simplifies when we represent the constant geometry of the modules using K_B^Q such that $H_{B_i}^{Q_i}(\theta_{Q_i}) = K_B^Q R_z(\theta_{Q_i})$ (note the lack of subscripts on K_B^Q indicates that "K" terms are the same for all modules). The redundancy in the revolute joints created by docked pairs can also be simplified noting $\rho(\alpha + \beta) = R_z(\alpha) D_0 R_z(-\beta)$ and $\rho(\alpha + \beta + \pi) = R_z(\alpha) D_\pi R_z(-\beta)$. Applying these newly defined relations to (3) yields:

$$\begin{aligned} &H_{P_1}^{L_6}(\theta_{P_1}, \theta_{C_1}, \theta_{C_2}, ...\theta_{L_6}) = \\ &\quad R_z(-\theta_{P_1}) K_P^C \rho(\theta_{C_1} + \theta_{C_2} + \pi) ... K_C^L R_z(\theta_{L_6}) \end{aligned} \tag{4}$$

Currently, the workspace of a given chain is defined iteratively using collision detection algorithms. This is done by checking all combinations of valid joint angles (from 0 to 360^o) discretized over a constant change in joint angle, $\Delta(\alpha + \beta)$ (e.g. $\Delta(\alpha + \beta) = 1.0^o$). Each time a configuration is found that does not result in a collision, the joint angles as well as the position and orientation of the

end-effector are added to an array. Once all combinations of joint angles are checked, this array can be used effectively as a lookup table both for determining whether desired end-effector positions and orientations are achievable, and for determining the various sets of joint angles associated with a given end-effector position and orientation (i.e. the inverse kinematics). A discussion of the shortcomings of using a string of characters to describe more complex assemblies, as well as the inefficiency associated with this iterative method of defining the workspace is in Section V.

B. Driving Kinematics

To create assemblies from individual modules, driving kinematics must be considered. Given the unique geometry of the module, the driving kinematics cannot be simply derived by imposing a no-slip condition on each wheel. The result of forcing the system to adhere to these conditions produces a module whose only feasible movement is to spin about its center wheel. To rectify this, the normal forces seen by each wheel during level driving are considered.

Assuming level driving, given module weight mg, with the center of mass located at the origin of Frame B (see Fig. 5), the normal force at each wheel is presented in (5).

$$\begin{aligned} N_P &= mg(L - l_P)/L \\ N_C &= mg(l_P W - L w_P)/(WL) \\ N_L &= mg w_P / W. \end{aligned} \tag{5}$$

Noting the relation $L = 2W$ mentioned in Section II-A, and center of mass location estimated at $l_p \approx \frac{2}{3}L$ and $w_p \approx \frac{1}{3}W$, the following relations emerge:

$$N_C > N_P, \;\; N_L > N_P, \;\; \text{and } N_C \approx N_L. \tag{6}$$

Further assuming a Coulomb friction model, with coefficient μ, is applicable to all wheels (i.e. $F_P \leq \mu N_P$, $F_C \leq \mu N_C$, etc.), we see that the dominant friction forces on the co-axial wheels cause the orthogonal wheel to slip during driving.

Noting this, the driving kinematics are derived by applying a no-slip condition to each of the coaxial wheels. The result, shown in (7), is dependent on $\theta_C(t)$ and $\theta_L(t)$ (the rotation about z_C and z_L respectively) and is equivalent to the equations of a classic kinematic cart offset to our body-fixed reference frame (Frame B). The variables $x(t)$ and $y(t)$ represent the position of the origin of Frame B projected onto the driving plane, and $\theta(t)$ represents the orientation of the module about the orthogonal axis.

$$\begin{pmatrix} \dot{x}(t) & \dot{y}(t) & \dot{\theta}(t) \end{pmatrix}^T = \frac{r}{W} \, G(\theta(t)) \begin{pmatrix} \dot{\theta}_C(t) & \dot{\theta}_L(t) \end{pmatrix}^T, \tag{7}$$

where $G(\,\theta(t)\,)$ is given in (8):

$$G(\,\theta(t)\,) = \begin{pmatrix} -w\ s(\theta(t)) + l\ c(\theta(t)) & -w_p\ s(\theta(t)) + l\ c(\theta(t)) \\ w\ c(\theta(t)) + l\ s(\theta(t)) & w_p\ c(\theta(t)) + l\ s(\theta(t)) \\ -1 & -1 \end{pmatrix}, \tag{8}$$

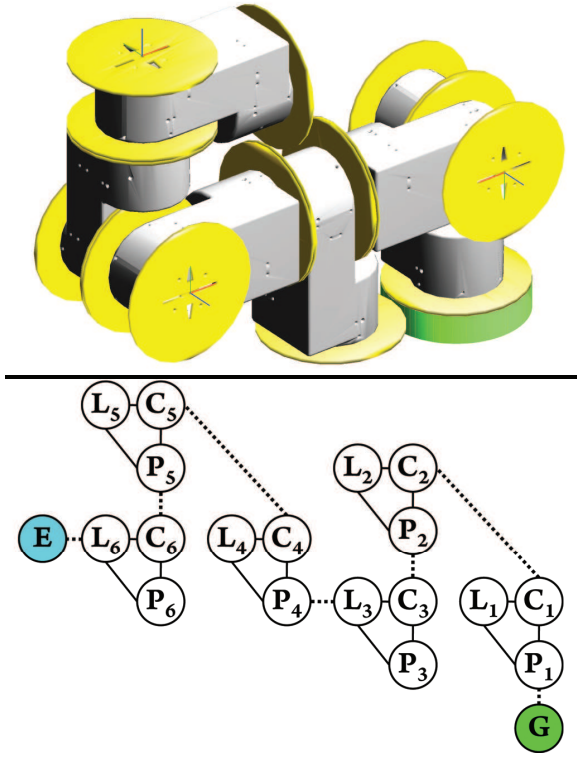

Fig. 6. Simulation of the "PCπCPπCLπPCπCPπCL" chain (top) and the graph representation of the structure (bottom).

and w and l are defined in (9):

$$w = w_p - W, \quad l = l_p - L. \tag{9}$$

An additional slip-minimizing constraint (10) can be added to the orthogonal wheel described by Frame P.

$$\dot{\theta}_P(t) = \frac{-L}{r}\dot{\theta}(t) \tag{10}$$

Note that, by using this slip-minimizing constraint, the perpendicular wheel is driven to match the rotational velocity of the module, resulting in slip that occurs only in the direction parallel to the axis of the perpendicular wheel. This allows the future possibility of replacing the (currently solid) perpendicular wheel with a holonomic drive wheel (containing orthogonal rollers) in order to eliminate slip altogether.

Using (7) and (10), maneuvers to dock two individual modules can be calculated. For example, a two individual module docking problem can be defined as follows: Given modules 1 and 2, connect C_1 to C_2 with docking orientation D_π. Initial configurations for each module are defined in terms of the body frame position and orientation, and docking wheel orientations. In this case:

$$\begin{aligned} &\text{Module 1 initial configuration:} \\ &\{x_1(t_0), y_1(t_0), \theta_1(t_0), \theta_{P_1}(t_0), \theta_{C_1}(t_0), \theta_{L_1}(t_0)\,\} \\ &\text{Module 2 initial configuration:} \\ &\{x_2(t_0), y_2(t_0), \theta_2(t_0), \theta_{P_2}(t_0), \theta_{C_2}(t_0), \theta_{L_2}(t_0)\,\} \end{aligned} \tag{11}$$

To simplify the problem, we assume one of the modules (for this example, module 2) remains stationary (i.e. $x_2(t_f) =$

$x_2(t_0)$, $\dot{x}_2(t) = 0$, $y_2(t_f) = y_2(t_0)$, etc.). This allows us to easily solve for the final configuration of module 1 ($x_1(t_f)$, $y_1(t_f)$, $\theta_1(t_f)$, and $\theta_{C_1}(t_f)$) in terms of the initial conditions.

With the initial and final configurations of module 1 defined, the next step is to address the nonholonomic motion planning problem where module 1's motion is constrained by (7). A more detailed description of this problem along with several viable solutions is presented in [15].

IV. PRELIMINARY EXPERIMENTAL RESULTS

A single, operational module has been fabricated, and preliminary testing has begun. Successful user-controlled docking between an operational module and a dummy module (a module matching the geometry and approximate weight but not containing electrical or mechanical components) was demonstrated with each of the three docking mechanisms. The docking and the initial motion test of the center wheel is shown in Fig. 7.

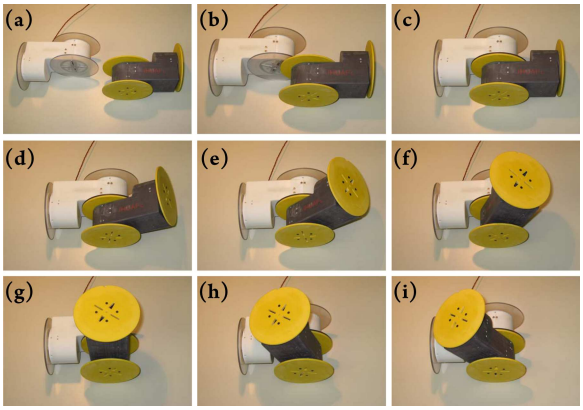

Fig. 7. Images taken from a successful docking and lifting test with an operational module (white), and a dummy module (black).

Lifting tests for two of the three wheels have also been performed. To do so, the body of the operational module is fixed to a table, and a simple test rig with a straight, rigid arm and known mass properties is connected to the tested wheel. The arm of the test rig is approximately aligned orthogonal to the gravitational field using a bubble level, and known weights are hung from the end of the arm. The operational module then lifts the applied load powered by an external power supply providing the nominal motor voltage, a constant 3.6V. While lifting, the motor current is carefully monitored. The peak currents for each of the applied torques are shown in Fig. 8. Based on the figure, the net efficiency of torque transmitted from the motor to the wheel is approximately 14.3%.

V. DISCUSSION

In this paper we presented the design, preliminary testing, and simulations of a new, self-mobile modular robot. The current module design meets our primary objective of creating a self-mobile unit capable of creating rigid assemblies and assemblies that facilitate negotiating rough/varied

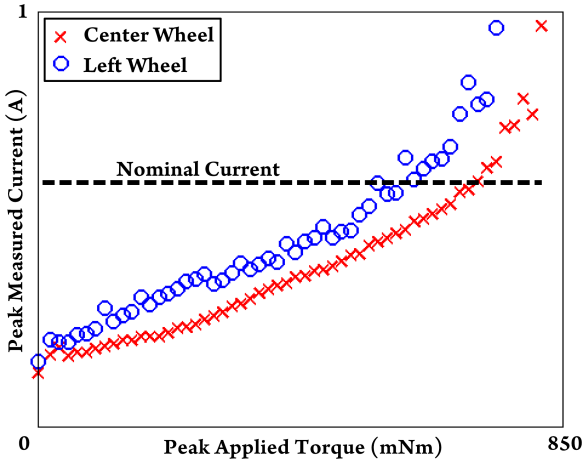

Fig. 8. Lifting test results for both the center and right wheel.

terrain. In addition, the current design meets each of the requirements stated in Section II, and the physical embodiment has demonstrated the design's feasibility.

To date we have created a single physically operational module, and one dummy module for preliminary evaluation. Early test results have been promising, and further testing is currently underway. Each of the operational module's three docking mechanisms work as expected, and docking has been demonstrated on each of the three wheels. In addition, the lifting capability of the two predominant lifting wheels (C and L) was tested, and the results are presented in Fig. 8.

While preliminary testing of our operational module has been promising, the current physical embodiment can still benefit from several improvements. The results in Fig. 8 show that torque is transmitted from the motor to the wheels with a net efficiency of approximately 14.3%. This corresponds to an ability to nominally lift a single module cantilevered perpendicular to the gravitational field with a safety factor of $>$1.96. When running near stall, this safety factor increases to $>$2.34. Despite these high values, we are yet unable to lift more than a single module without improving the efficiency of our gear train.

To do so, we consider the following improvements prior to future testing and/or prior to building future robots: (1) Identification of a better dry, non-electrically conductive lubricant for use on open gear assemblies within the module. (2) The addition of more precise alignment features for assembling the worm/worm gear combination. (3) Weight reduction by replacing conservatively specified brass and steel gears with gears made of a lighter material (e.g. aluminum alloy or plastic). By implementing these improvements, we anticipate lifting capabilities equal to or better than those described in Section II-A.

There are currently no standard benchmarks for modular robot performance. As such, it is difficult to directly compare mechanical performance between different systems. In some cases a test scenario is explicitly described (e.g. [7] describes a module-lift test for MTRAN, and [1] lists a max cantilever module value of 5 for Polybot), while in other cases only

more general performance data is presented. It is also not always clear if the reported values are engineering estimates or results of actual measurements. Nevertheless, we can compare the performance of our modules with a best estimate of other systems based on reported values. The mass of our module is approximately 800 grams, and the maximum measured output torque of the lifting axis is 0.814 Nm. This compares with the following values for other systems: Conro [3]: 114g, 0.36 Nm; Atron [6]: 825g, 2.36 Nm; MTRAN II [12]: 400g, 1.9 Nm; SuperBot [10]: 878g, 6.38 Nm. With the improvements described in (1)-(3), we hope to achieve the following values for future modules: 600g, 4.6 Nm.

As discussed in Section I, one application for these modular robots involves the temporary reconstruction of power lines. Since the docking hooks are made from conductive material, power can be routed between modules using the hooks as connection points. However, since the final configuration of multiple modules in a given scenario may not be known a priori, it is necessary to have the capability to alter the electrical connectedness of individual hooks on the fly. In future prototypes, this will be accomplished through internal relays within each module. The relays will allow power, ground, and other signals to be routed between modules in any desired configuration.

In Section III-A, we note that our current method of defining the workspace of chain assemblies is inherently inefficient. For any given chain we step through all possible joint configurations without considering the kinematics of chains contained within the larger assembly. Put more precisely, the chain "PCπCPπCLπPCπCPπCL" simulated in Fig. 6 contains the chain "PCπCPπCLπPCπCP". Likewise, the chain "PCπCPπCLπPCπCP" contains the chain "PCπCPπCLπPC", "PCπCPπCLπPC" contains "PCπCPπCL", etc. A possible improvement to our current algorithm might be to first define the workspace of the simple chains contained within the larger assembly. We can then use this workspace information to limit the set of joint configurations that we explore in the larger assemblies thereby reducing the total number of required iterations. Further investigation into this topic will be address in future work.

When trying to define more complex assemblies such as closed loops and trees (as required in the formation of lattice structures), we immediately note that our current method of defining chains is insufficient. Future work will focus on characterizing assemblies using methods similar those presented in [16]. To do so, we can define a node or vertex for each frame illustrated in Fig. 5. Nodes are labeled using the character that defines the frame (Frame P_i corresponds to Node P_i, Frame C_i corresponds to Node C_i, etc.). A graph representation of the "PCπCPπCLπPCπCPπCL" chain is illustrated in Fig. 6. Here, we introduce nodes G and E to represent the ground and end-effector locations. The solid edges are used to represent permanent connections within modules, while dashed edges represent connections that can be broken. Unlike our current method, the use of graph representations and/or representations using an adjacency matrix provide a more straightforward method for defining closed loops and trees.

VI. ACKNOWLEDGMENTS

The authors thank Dr. Kiju Lee, Jason Glasser, and Kevin Wolfe for their contributions to this project. This work was supported by Internal Research and Development funds provided by the Johns Hopkins University Applied Physics Laboratory and by NSF grant IIS-0915542, RI: Small:Robotic Inspection, Diagnosis, and Repair.

REFERENCES

[1] M. Yim, W.-M. Shen, B. Salemi, D. Rus, M. Moll, H. Lipson, E. Klavins, and G. Chirikjian, "Modular self-reconfigurable robot systems [Grand Challenges of Robotics]," *IEEE Robot. Autom. Mag.*, vol. 14, no. 1, pp. 43–52, Mar. 2007.

[2] S. Murata and H. Kurokawa, "Self-reconfigurable robots: Shape-changing cellular robots can exceed conventional robot flexibility," *IEEE Robot. Autom. Mag.*, pp. 71–78, Mar. 2007.

[3] A. Castano, A. Behar, and P. M. Will, "The Conro modules for reconfigurable robots," *IEEE/ASME Trans. Mechatronics*, vol. 7, no. 4, pp. 403–409, Dec. 2002.

[4] M. Yim, B. Shirmohammadi, J. Sastra, M. Park, M. Dugan, and C. Taylor, "Towards robotic self-reassembly after explosion," in *Proceedings of the 2007 IEEE/RSJ International Conference on Intelligent Robots and Systems*, 29 2007-Nov. 2 2007, pp. 2767–2772.

[5] D. Rus and M. Vona, "A basis for self-reconfiguring robots using crystal modules," in *Proceedings of the 2000 IEEE/RSJ International Conference on Intelligent Robots and Systems*, 2000, pp. 2194–2202.

[6] M. Jorgensen, E. Ostergaard, and H. Lund, "Modular ATRON: modules for a self-reconfigurable robot," in *Intelligent Robots and Systems, 2004. (IROS 2004). Proceedings. 2004 IEEE/RSJ International Conference on*, vol. 2, 2004, pp. 2068–2073.

[7] S. Murata, E. Yoshida, K. Tomita, H. Kurokawa, A. Kamimura, and S. Kokaji, "Hardware design of modular robotic system," in *Proceedings of the 2000 IEEE/RSJ International Conference on Intelligent Robots and Systems*, 2000, pp. 2210–2217.

[8] W.-M. Shen, "Self-reconfigurable robots for adaptive and multifunctional tasks," in *Proceedings of the 26th Army Science Conference*, Florida, USA, Dec. 2008.

[9] S. Murata, K. Kakomura, and H. Kurokawa, "Docking experiments of a modular robot by visual feedback," in *Proceedings of the 2006 IEEE/RSJ International Conference on Intelligent Robots and Systems*, Oct. 2006, pp. 625–630.

[10] F. Hou, N. Ranasinghe, B. Salemi, and W.-M. Shen, "Wheeled locomotion for payload carrying with modular robot," in *Proceedings of the 2008 IEEE/RSJ International Conference on Intelligent Robots and Systems*, Sep. 2008, pp. 1331–1337.

[11] V. Zykov, A. Chan, and H. Lipson, "Molecubes: An open-source modular robotics kit," in *IROS-2007 Self-Reconfigurable Robotics Workshop*, 2007. [Online]. Available: http://www.molecubes.org/

[12] A. Kamimura, H. Kurokawa, E. Yoshida, S. Murata, K. Tomita, and S. Kokaji, "Automatic locomotion design and experiments for a modular robotic system," *IEEE/ASME Trans. Mechatronics*, vol. 10, no. 3, pp. 314–325, Jun. 2005.

[13] K. Kotay and D. Rus, "Efficient locomotion for a self-reconfiguring robot," in *Proceedings of the 2005 IEEE International Conference on Robotics and Automation*, Apr. 2005, pp. 2963–2969.

[14] G. S. Chirikjian, "Metamorphic hyper-redundant manipulators," in *Proceedings of the 1993 JSME International Conference on Advanced Mechatronics*, Aug. 1993, pp. 467–472.

[15] K. C. Wolfe, M. D. M. Kutzer, M. Armand, and G. S. Chirikjian, "Trajectory generation and steering optimization for self-assembly of a modular robotic system," in *Proceedings of the 2010 IEEE International Conference on Robotics and Automation*, May 2010, In Press.

[16] M. Park, S. Chitta, A. Teichman, and M. Yim, "Automatic configuration recognition methods in modular robots," *The International Journal of Robotics Research*, vol. 27, pp. 403–421, Mar. 2008.